SAND2022-17086C

Shock-Particle Curtain Interactions at High Mach Number

Justin L. Wagner[1], Kyle A. Daniel[2], Charley R. Downing[3], and Kyle P. Lynch[2]
Sandia National Laboratories, Albuquerque, NM

Shock-particle interactions at elevated Mach numbers are studied using the Sandia free-piston High-Temperature Shock Tube (HST). Like previous studies in a lower-strength facility, the particle curtain was comprised of 100-micron glass at an initial volume fraction of approximately 20%. Shock-particle interactions were investigated using high-speed imaging, where the incident shock Mach number ranged from 3 – 4.2. The corresponding post-shock velocities were 760 – 1170 m/s, nearly doubling the range available in previous experiments. The spread of the particle was curtain compared to that in the literature. The scaling law of DeMauro et al. (2019) effectively collapsed the curtain spread over experiments ranging approximately one order of magnitude of post-shock velocities.

I. Introduction

Shock-particle interactions produce compressible, multiphase flows important to several engineering applications including heterogeneous explosives [1], pulsed detonation engines [2], mining safety [3], and rocket propulsion [4]. An important parameter in such flows is the particle volume fraction φ_p, which dictates the dynamics of shock-particle interactions. In the dense regime, where φ_p resides between about 0.1% and 50%, the exchange of momentum between the solid and gas phases is poorly understood [1]. This has motivated previous experiments on the dispersal of particle curtains in shock tubes having volume fractions of 9 – 32% [5-8], which have inspired several modeling campaigns [9-15]. Ling et al. [9] suggest that dense volume fractions increase both quasi-steady drag and lead to prolonged unsteady effects which serve to enhance the interphase momentum transfer in comparison to standard drag laws. Theofanous et al. [6], DeMauro et al. [7], and Daniel and Wagner [16] report that a dominant effect is the pressure gradient across the curtain, which is initiated by the reflection of the incident shock off the initially stationary particles. In all experiments, the dense volume fractions lead to a rapid spread of the particle curtain, which exhibits a bulk translation faster than that predicted with standard drag laws [17].

A dimensional analysis was utilized by Thefanous et al. [12] to scale time as a function of the reflected shock pressure by treating the curtain as a solid wall. Building upon this, control volume analyses were used by Daniel and Wagner [16] and DeMauro et al. [8] to suggest the following scaling relationships:

$$\frac{x}{\delta_0} = \left(\frac{\sqrt{\Delta P}t}{\sqrt{\rho_p}\delta_0}\right)^2, \tag{1}$$

$$\frac{x}{\delta_0} \propto \left(\psi_p^{0.25}\sqrt{\frac{\rho_p}{\rho_0}}\frac{U_{ind}t}{\delta_0}\right)^2 = (t^*)^2, \tag{2}$$

where ΔP is the curtain-induced pressure gradient, ρ_p is the particle density, ρ_0 is the initial gas density, and U_{ind} is the velocity following the incident shock. Note that Equation (1) is similar to the Theofanous scaling except the pressure difference here corresponds to the actual value as opposed to a theoretical reflected shock. Daniel and Wagner [16] demonstrated tight collapse of the particle curtain spread using equation (1) and the pressures measured across the curtain over a range of volume fractions. This is because the porosity directly alters the strength of the reflected and transmitted shocks and thus the pressure gradient across particle curtain. In contrast, the time normalization in Equation (2) stems from modeling the pressure drop across the particle curtain as a porous screen and incorporates only initial parameters known prior to the experiment.

The experimental parameters for a variety of shock-particle curtain interaction experiments are summarized in Table 1. The previous studies span a wide range of ψ_p, ρ_p, particle diameter d_p, δ_0, incident shock Mach number M_s, and therefore, U_{ind}. DeMauro et al. [8] showed a tight collapse of curtain spread for varying volume fractions at constant particle density using the nondimensional time t^* in Equation (2). Similarly, Daniel and Wagner [16] tested

1 – Principal Member of the Technical Staff, Engineering Sciences Center. Associate Fellow AIAA: jwagner@sandia.gov
2 – Senior Member of the Technical Staff, Engineering Sciences Center. Member AIAA
3 – Principal Technologist, Engineering Sciences Center

the same scaling showing tight collapse of their own data while varying particle density by about one order of magnitude.

Table 1: Comparison of Experimental Parameters in Shock-Particle Interaction Studies

Reference	Ψ_p, %	ρ_p, kg/m^3	d_p, μm	δ_0, mm	M_s	U_{ind}, m/s
Ling et al. (2012)	21	2.4	106-125	2.0	1.7-2.0	300-440
Theofanous et al. (2016)	32	2.4	910	23-31	1.2-**2.6**	110-**630**
DeMauro et al. (2019)	9, 23	2.4	106-125, 300-355	1.8-3.0	1.2-1.5	120-220
Daniel and Wagner (2022)	9, 17-19	2.4-17.1	106-125, 300-355	1.6-3.9	1.4-1.7	210-330
Current Study	19-20	2.4	106-125	2.0	**3.0-4.2**	**760-1170**

Despite these gains in physical understanding, previous experiments have been limited to incident shock Mach numbers less than 2.6, which corresponds to post-shock flow velocities of 630 m/s. As a result, much of the data on dense, multiphase flows in shock tubes has been limited to conditions exceeded in research applications. The current work studies shock-particle interactions in the Sandia high-temperature shock tube (HST). The HST has a free-piston driver and can produce shock-induced velocities greater than 1.5 km/s using only the incident shock wave. Importantly, these conditions are generated when the driven section is at ambient pressure and temperature as in explosive environments. Like the first shock-particle curtain interaction experiments [5], the present apparatus uses a gravity-fed mechanism to produce dense volume fractions.

The present paper describes the HST apparatus including the particle curtain test section able to withstand high pressures. Particle curtain experiments using glass spheres are reported as M_s is varied from 3.0 – 4.2. The post-shock gas velocities span from 760 – 1170 m/s to double the range in the present literature (Table 1). ψ_p is approximately 20%. Here, the applicability of existing scaling laws is evaluated at such extreme conditions and compared to the entire set of shock-particle curtain data available in the literature.

II. Experimental Setup

A. HST

Description

Details on the free-piston shock tube are given in Lynch et al. [18] and are only briefly summarized here. The design of the HST (Fig. 1) is much like that in the University of Queensland X2 expansion tube [19]. A reservoir section filled with house nitrogen, typically at pressures of 700 – 2800 kPa, is used to launch a 35-kg piston down the driver. The driver section has a length of 5.2 m and an inner diameter of 0.267 m. The driven section is composed of modular sections and has a total length of ≈ 9 m and an inner diameter of 0.087 m. A 'sliding joint' between the reservoir and driver allows the driver and driven sections to translate freely during a shot mitigating the transmission of recoil forces into the reservoir section.

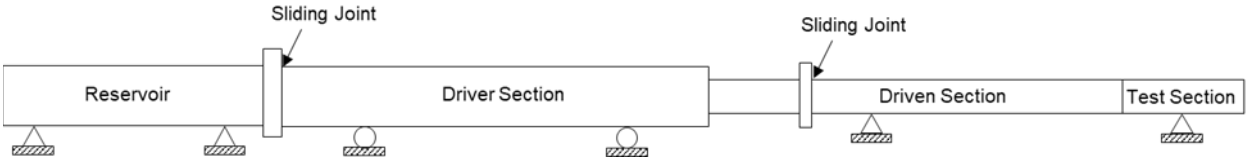

Fig. 1 Schematic of the HST.

Before an experiment, a vacuum is applied to both the driver and driven sections. Both sections are then backfilled to prescribed pressures and gas compositions. The piston is initially held in place with a vacuum acting on the back face of the piston. During a shot, a three-way-valve is actuated removing the vacuum from the back face of the piston and instead exposing this face to the high pressure in the reservoir. This effectively launches the piston, which is propelled at several hundred m/s. Tens of milliseconds (ms) later, the piston reaches the end of the driver, the driver gas is compressed to a small volume, and the diaphragm bursts. Diaphragms made from carbon steel are cruciform scored in-house, and the driver burst pressure is set by the diaphragm thickness and score depth.

Early particle curtain experiments in HST had an initially perturbed curtain with a 'wavy' shape due to the recoil of the facility associated with launching the piston down the driver [20]. During a shot, the facility moves about 25 mm upstream followed by 100 mm of downstream travel. The HST now includes a second sliding joint (Fig. 1), which

effectively isolates the motion of the driver from the driven section, test section, and particle curtain. Briefly, the design is like that of Gilfind and Morgan [21] and results in minimal disturbance to the incident shock and particle curtain.

High-Speed Pressure Measurements

A fast-response PCB pressure sensor (Model 113B122, range of 34.5 MPa) is used to monitor the driver pressure during this process. Similar pressure sensors are placed within the driven section to monitor shock speed and pressure. The PCB signals pass through a signal conditioner (PCB Model 483C) that provides the transducers the constant current and the excitation voltage necessary for operation while it also amplifies the sensor signals. The amplified signals are then low-pass filtered (Krohn-Hite Model 3384) with a cutoff frequency of 400 kHz. The filtered signals are sent to a data acquisition chassis, in which two 14-bit data acquisition cards digitize the signals at a sampling frequency of 800 kHz before being recorded on a personal computer.

Experimental Conditions

In comparison to standard shock tubes, the free-piston driver allows for very strong shock waves. The isentropic compression process serves to simultaneously pressurize the driver to ≈ 24 MPa while simultaneously heating it to ≈ 2000 K. The conditions for the present particle curtain experiments are listed in Table 2. The incident shock Mach number M_s is measured using crossing times from pressure sensors ≈ 50 mm and 300 mm upstream of the test section and has an uncertainty of about 2%. Post-shock conditions U_{ind}, pressure P_2, and density ρ_2 are calculated using the NASA Chemical Equilibrium with Applications (CEA) code [22]. In all cases the driven gas is air at an initial pressure P_1 of about 83.4 kPa (ambient pressure), the curtain is comprised of soda-lime glass particles having diameters sieved to 106 – 125 μm, φ_p is ≈ 20%, and δ_0 is 2 mm. The experiments span a U_{ind} range of 760 – 1170 m/s, which is controlled in part by varying the driver gas from 100% argon to a 70-30% helium-argon mix.

Table 2: Experimental Conditions

Run, #	Ψ_p, %	Material	ρ_p, kg/m^3	δ_0, mm	M_s	U_2, m/s	P_2, bar	T_2, K
228	19	soda-lime glass	2.42	2.0	2.97	762	8.6	764
229	19	soda-lime glass	2.42	2.0	3.56	955	12.4	969
233	19	soda-lime glass	2.42	2.0	4.24	1173	17.8	1236

B. Particle Curtain Test Section

Design

The particle curtain test section having a length of 381 mm is shown in Fig. 2. To accommodate optical diagnostics, it has a square cross-section of width 73.2 mm. Two square sections of identical width and length precede the test section, each instrumented with a PCB pressure sensor (Fig. 2a). Each square section, including the test section, is fabricated from a billet of high-strength stainless steel (alloy 17-4PH condition H1150M). The internal machining was achieved via a wire electric discharge machine. A section upstream of the square section smoothly transitions from the circular cross-section of the baseline HST. The area is maintained between the circular and square sections to minimize disturbances to the incident shock. At the upstream end, the new hardware attaches to the round pipe of the HST with a Grayloc pipe connector. An additional square section can be added downstream of the test section (Fig. 2b) to delay the arrival of the reflected shock if necessary.

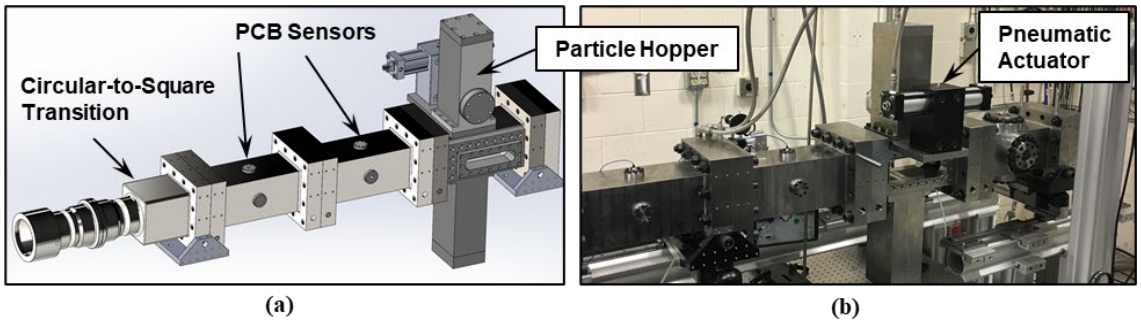

Fig. 2 Particle curtain test section: (a) illustrative schematic, and (b) photo.

A beveled slit, like that used in previous particle curtain experiments in the multiphase shock tube (MST) [5, 9, 16], fits into a pocket on the test section ceiling. The slit spans the entire test section width and has a streamwise thickness of 3.2 mm. Activation of a pneumatic actuator (Fig. 2) begins the flow of particles from the particle hopper into the test section. The shaft rotates within a stationary sleeve made from hardened tool steel, which fits into the hopper. This sleeve has a slot that is aligned with the slot in the hopper holding the particles. The rotary shaft has a slot with equivalent area that is rotated to be in line with that of the hopper and sleeve upon actuation to allow particle flow. This functionality is like that of a standard ball valve. The particles exit the test section into a particle reservoir through a slit of equivalent area. High-pressure tubing connects the hopper and reservoir section to provide pressure equalization and a clean particle flow. The flow of particles begins about 0.5 seconds prior to firing the shock tube to ensure the curtain has reached steady state. Cast-acrylic, elliptical windows having a viewing area of approximately 169 mm × 38 mm attach to the section sidewalls. Extensive scratching occurs during the strong shock-particle curtain interactions in HST. The acrylic material is chosen to make window replacement between runs more affordable.

Particle Curtain Characterization

During a shock tube experiment, the curtain is monitored with a Phantom high-speed color camera at a framing rate of 500 Hz to ensure proper particle flow. Upon actuation of the rotary mechanism, it takes about 0.2 seconds for the particle flow to stabilize. The resulting particle curtain spans the width of the test section (Fig. 3a) and has a streamwise thickness of 2 mm (Fig. 3b). To compare to the previous work in the MST [5], the curtain is shaped from soda-lime spherical particles sieved to a size distribution of 106 – 125 micrometers. The particle volume fraction is calculated as previously [5, 7]. Briefly, the mass flow rate of the curtain is measured using a load cell. The cross-sectional area of the curtain is taken as the test section width × curtain streamwise thickness. The particle velocity is taken to be that given by gravitational acceleration [7]. With the known mass flow rate, particle velocity and occupied area, a density of the glass-air mixture is determined. This allows for the volume fraction to be determined. Involved here is a simplifying assumption that the streamwise volume fraction distribution exhibits a top hat profile. Previous modeling and X-ray measurements have shown that profile is in fact Gaussian [17, 23]. Nevertheless, the top-hat assumption gives a simple way to characterize volume fraction over a range of facilities without the need for complex X-ray measurements. In the present case, the volume fraction comes to 20% at mid-height, the same as in previous MST experiments using a similar beveled-slit geometry and soda-lime particle size distribution.

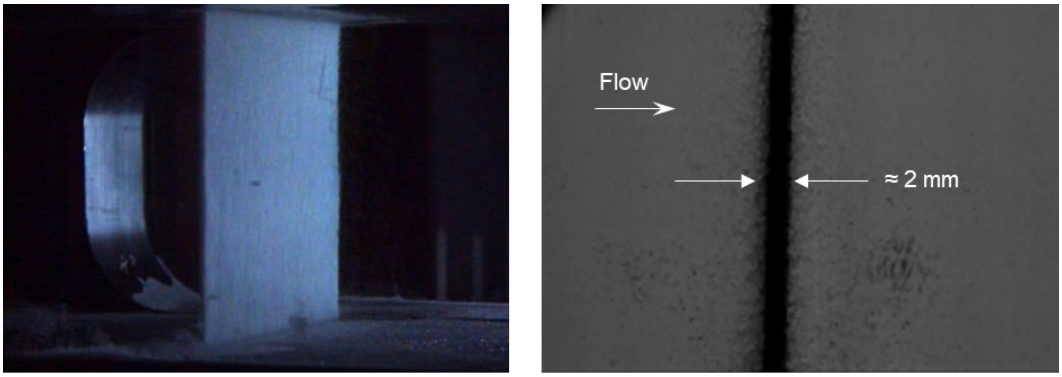

Fig. 3 Particle curtain in the HST: (a) photo showing the entire height of the curtain within the test section from a 500 frame-per-second video and (b) schlieren image of the curtain before an experiment.

C. High-Speed Shadowgraph Imaging System

A high-speed shadowgraph imaging system was used to study the shock-particle interactions. The light source was a Cavitar pulsed laser diode (Cavilux Smart UHS) operated at a frequency of 300 kHz, a pulse width of 10 ns, and a wavelength of approximately 630 ± 10 nm. The images were acquired with a Phantom digital camera (TMX 7510) having a resolution at full frame of 1280 × 800 pixels. The framing rate was 300 kHz, the image resolution was 684 × 340 pixels, and the image exposure time was 1 microsecond. To collimate the source, a 100-mm diameter planoconvex lens with a focal length of 1 m was used. A similar lens focused the light onto the camera. Special care was taken to align the imaging system normal to the test section to minimize errors associated with off-normal incident light [24]. The positions of the upstream and downstream fronts of the curtain are taken to be the location where the pixel intensity reaches 5% of that in the particle-free background [9, 16].

III. Results

A. Shock-Particle Curtain Interaction in the HST

Results are presented as function of time and normalized time t^* per Equation (2). The first 140 μs ($t^* = 1.11$) of a Mach 4.2 shock-particle interaction are shown in Fig. 4. The images correspond to Run 233 (Table 2) where the post-shock velocity is 1170 m/s and the particles are soda-lime glass. At $t^* = -0.05$ (Fig. 4a), the incident shock has propagated to just upstream of the particle curtain. Unlike previous work in the HST with a 'wavy' curtain [20], the particle distribution here is vertically straight and shows much less influence of the facility recoil. By $t^* = 0.16$ (Fig. 4b), a transmitted and reflected shock are seen propagating downstream and upstream, respectively. These shocks occur following the impingement of the shock on the curtain. The flow downstream of the transmitted shock has significant density gradients associated with turbulence. Particle-resolved direct numerical simulation (PR-DNS) of shock-particle cloud interactions suggests the flow features are associated with the unsteady waves and wakes during the impulsive start of the curtain flow [25]. Such multiphase effects are defined as pseudo-turbulence [13]. With continuing time (Fig. 4c), the transmitted and reflected waves continue to propagate. A net downstream propagation and spread of the current is apparent. At $t^* = 1.11$ (Fig. 4d), the shocks have left the field-of-view and there is a substantial increase in the spread of the curtain. The spread of the curtain is used to subsequently evaluate scaling laws at the elevated shock Mach numbers provided by the HST.

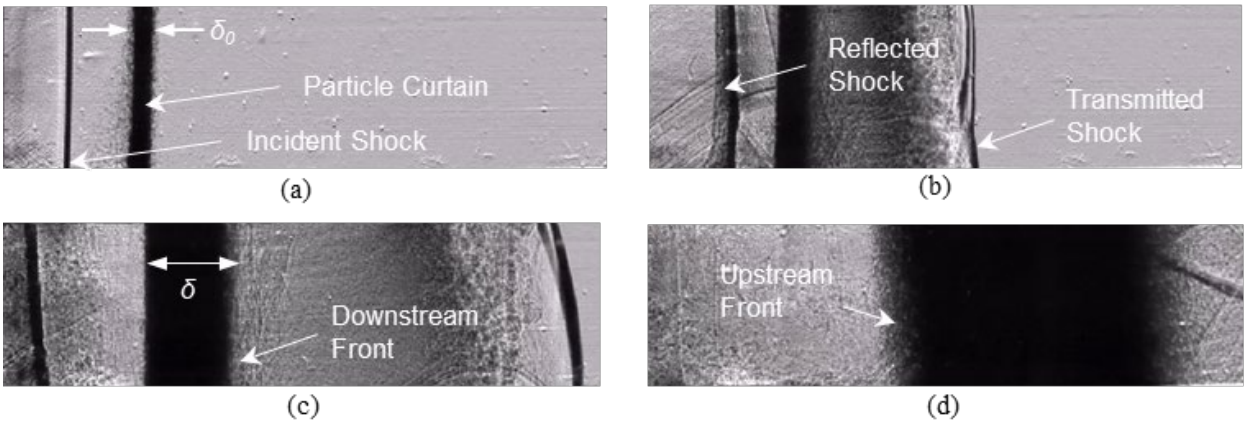

Fig. 4 High-speed imaging sequence obtained during a Mach 4.2 shock-particle curtain interaction at t^*: (a) -0.05 (t = -6.7 μs), (b) 0.16 (t = 20 μs), (c) 0.42 (t = 53.3 μs), and (d) 1.11 (t = 140 μs).

B. Application of Scaling Laws

The non-dimensional particle curtain spread for all three conditions is shown in Fig. 5. In each case, residual recoil through the test section thickens the curtain by about 25% after the shock tube is fired, but prior to arrival of the incident shock. Here δ_0 and ψ_p are taken to be the pre-shot values. The curtain spread as a function of time (Fig. 5a) shows expected trends, namely that the glass and that particles spread faster at higher M_s and U_{ind}. A tight collapse is observed when the trajectories are plotted versus t^* (Fig. 5b). Moreover, the constant δ [8], constant acceleration region (CAR), and constant velocity region CVR [12] region are readily observed in the scaled HST data.

Data from historical particle curtain experiments (Table 1) are compared to the current high-speed HST results in Fig. 6. The dependence of δ/δ_0 on these parameters is captured in Fig. 6a where the trends of faster particle spread with increasing M_s and decreasing ρ_p are clear. The experiments of Theofanous et al. [6] have larger δ_0 and spread at a much slower rate than the rest. Also evident is the faster spread of the curtain with increasing ψ_p consistent with a larger pressure gradient and quasi-steady drag. The scaled results in Fig. 6b shows strong collapse of the curtain spread over one order of magnitude of U_{ind} (110-1170 m/s), δ_0 (1.8-33.5 mm), and ρ_p (2.4-17.1 kg/m), whereas the volume fraction varies from 0.09-0.32. Importantly, the particle diameter is not included in the scaling, though it also varies by ≈ one order of magnitude (105-905). This suggests that the dynamics of the shock-induced dispersal are dominated by bulk phenomena within the curtain as it expands as opposed to the dynamics of individual particle interactions.

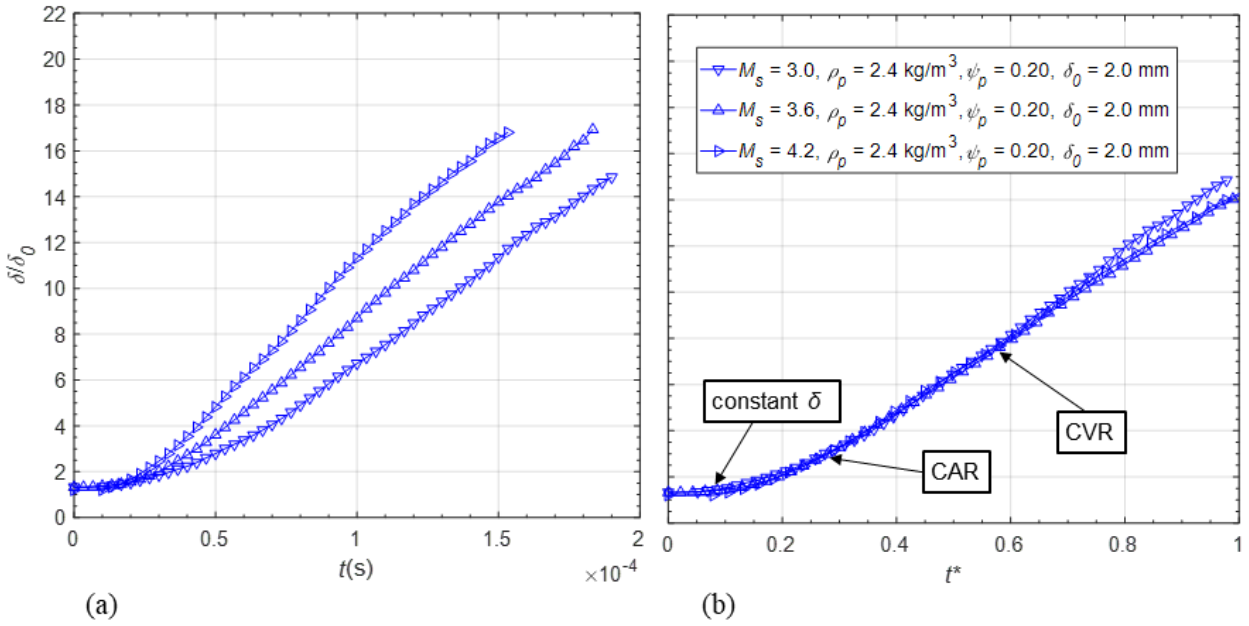

Fig. 5 Particle curtain spread in the HST: (a) non-dimensional spread δ/δ_0 versus time, and (b) δ/δ_0 versus t^*.

Acknowledgements

The authors would like to thank Paul Farias for design of the section hardware. Sandia National Laboratories is a multi-mission laboratory managed and operated by National Technology & Engineering Solutions of Sandia, LLC, a wholly owned subsidiary of Honeywell International Inc., for the U.S. Department of Energy's National Nuclear Security Administration under contract DE-NA0003525. This paper describes objective technical results and analysis. Any subjective views or opinions that might be expressed in the paper do not necessarily represent the views of the U.S. Department of Energy or the United States Government.

References

[1] Zhang, F., Frost, D. L., Thibault, P. A., Murray, S. B. "Explosive Dispersal of Solid Particles," *Shock Waves*, Vol. 10, No. 6, 2001, pp. 431-443.

[2] Kailasanath, K., "Liquid-Fueled Detonations in Tubes," *Journal of Propulsion and Power*, Vol. 22, No. 6, 2006, pp. 1261-1268.

[3] Merzkirch, W. and Bracht, K., "The Erosion of Dust by a Shock Wave in Air: Initial stages with Laminar Flow," *International Journal of Multiphase Flow*, Vol. 4, No. 1, 1978, pp.89-95.

[4] Davis, S. L., Dittmann, T. B., Jacobs, G. B., and Don, W. S., "Dispersion of a Cloud of Particles by a Moving Shock: Effects of the Shape, Angle of Rotation, and Aspect Ratio. *Journal of Applied Mechanics and Technical Physics*, *54*(6), 2013, pp. 900-912.

[5] Wagner, J. L., Beresh, S. J., Kearney, S. P., Trott, W. M., Castaneda, J. N., Pruett, B. O., and Baer, M. R. "A Multiphase Shock Tube for Shock Wave Interactions with Dense Particle Fields, *Experiments in fluids*, Vol. 52, No. 6, 2012, pp. 1507-1517.

[6] Theofanous, T. G., Mitkin, V., and Chang, C. H., "The Dynamics of Dense Particle Clouds Subjected to Shock Waves Part 1. Experiments and Scaling Laws," *Journal of Fluid Mechanics*, Vol. 792, 2016, pp. 658-681.

[7] DeMauro, E. P., Wagner, J. L., Beresh, S. J., and Farias, P. A., "Unsteady Drag Following Shock Wave Impingement on a Dense Particle Curtain Measured using Pulse-Burst PIV," *Physical review fluids*, Vol. 2, No. 6, 2017, pp. 064301.

[8] DeMauro, E.P., Wagner, J. L., DeChant, L J., Beresh, S. J. and Turpin, A. M., "Improved Scaling Laws for the Shock-Induced Dispersal of a Dense Particle Curtain," *Journal of Fluid Mechanics*, Vol. 876, 2019, pp.881-895.

[9] Ling, Y., Wagner, J. L., Beresh, S. J., Kearney, S. P., and Balachandar, S., "Interaction of a Planar Shock Wave with a Dense Particle Curtain: Modeling and Experiments, *Physics of Fluids*, Vol. 24, No. 11, pp. 113301.

[10] Regele, J. D., Rabinovitch, J., Colonius, T., and Blanquart, G., "Unsteady Effects in Dense, High Speed, Particle Laden Flows," *International Journal of Multiphase Flow*, Vol. 61, 2014, pp. 1-13.

[11] Houim, R. W. and Oran, E. S., A Multiphase Model for Compressible Granular–Gaseous Flows: Formulation and Initial Tests, *Journal of Fluid Mechanics*, Vol. 789, 2016, pp. 166-220.

[12] Theofanous, T. G. and Chang, C. H., "The Dynamics of Dense Particle Clouds Subjected to Shock Waves. Part 2. Modeling/Numerical Issues and the Way Forward, *International Journal of Multiphase Flow*, vol. 89, 2018, pp. 177-206.

[13] Shallcross, G. S., Fox, R. O. and Capecelatro, J., "A Volume-Filtered Description of Compressible Particle-Laden Flows," *International Journal of Multiphase Flow*, Vol. 122, 2020, pp. 103138.
[14] Mehta, Y., Neal, C., Jackson, T. L., Balachandar, S. and Thakur, S., "Shock Interaction with Three-Dimensional Face Centered Cubic Array of Particles," *Physical Review Fluids*, Vol. 1, No. 5, 2016, p.054202.
[15] Mehta, Y., Neal, C., Salari, K., Jackson, T. L., Balachandar, S. and Thakur, S., "Propagation of a Strong Shock over a Random Bed of Spherical Particles," *Journal of Fluid Mechanics*, Vol. 839, 2018, pp.157-197.
[16] Daniel, K. A. and Wagner, J. L., "The Shock-Induced Dispersal of Particle Curtains with Varying Material Density," *International Journal of Multiphase Flow*, Vol. 152, 2022, p.104082.
[17] Wagner, J. L., Kearney, S. P., Beresh, S. J., DeMauro, E. P. and Pruett, B. O., "Flash X-Tay Measurements on the Shock-Induced Dispersal of a Dense Particle Curtain," *Experiments in Fluids*, Vol. 56, No. 12, 2015, p.p. 213.
[18] Lynch, K. P., Grasser, T. G., Spillers, R. W., Downing, C. J., Daniel, K. A., Jans, E. R., Kearney, S. P., Morreale, B. J., Wagnild, R. M., and Wagner, J. L., "Design and Characterization of the Sandia Free-Piston Shock Tunnel," under review in *Shock Waves*.
[19] C. Doolan, "Design and Construction of the X2 Two-Stage Free Piston Driven Expansion Tube," University of Queensland, 1995.
[20] Petter, S. J., Lynch, K. P., Farias, P., Spitzer, S., Grasser, T., & Wagner, J. L., "Early Experiments on Shock-Particle Interactions in the High-Temperature Shock Tube," In *AIAA Scitech*, 2020, Paper 2020-0622.
[21] Gildfind, D. E. and Morgan, R. G., "A New Sliding Joint to Accommodate Recoil of a Free-Piston-Driven Expansion Tube Facility, *Shock Waves*, Vol. 26, No. 6, 2016, pp.825-833.
[22] NASA. [Online]. Available: https://www.grc.nasa.gov/www/CEAWeb/ceaHome.htm.
[23] Goetsch, R. J. and Regele, J. D., "Discrete Element Method Prediction of Particle Curtain Properties," *Chemical Engineering Science*, Vol. 137, 2015, pp.852-861.
[24] Nili, S., Park, C., Kim, N. H., Haftka, R. T. and Balachandar, S., "Prioritizing Possible Force Models Error in Multiphase Flow using Global Sensitivity Analysis." AIAA Journal, Vol. 59, No. 5, 2021, pp.1749-1759.
[25] Hosseinzadeh-Nik, Z., Subramaniam, S. and Regele, J. D., "Investigation and Quantification of Flow Unsteadiness in Shock-Particle Cloud Interaction," *International Journal of Multiphase Flow*, Vol. 101, 2018, pp.186-201.
[26] Mehta, Y., Goetsch, R. J., Vasilyev, O. V. and Regele, J. D., "A Particle Resolved Simulation Approach for Studying Shock Interactions with Moving, Colliding Solid Particles," *Computers & Fluids*, Vol. 248, 2022, p.105670.

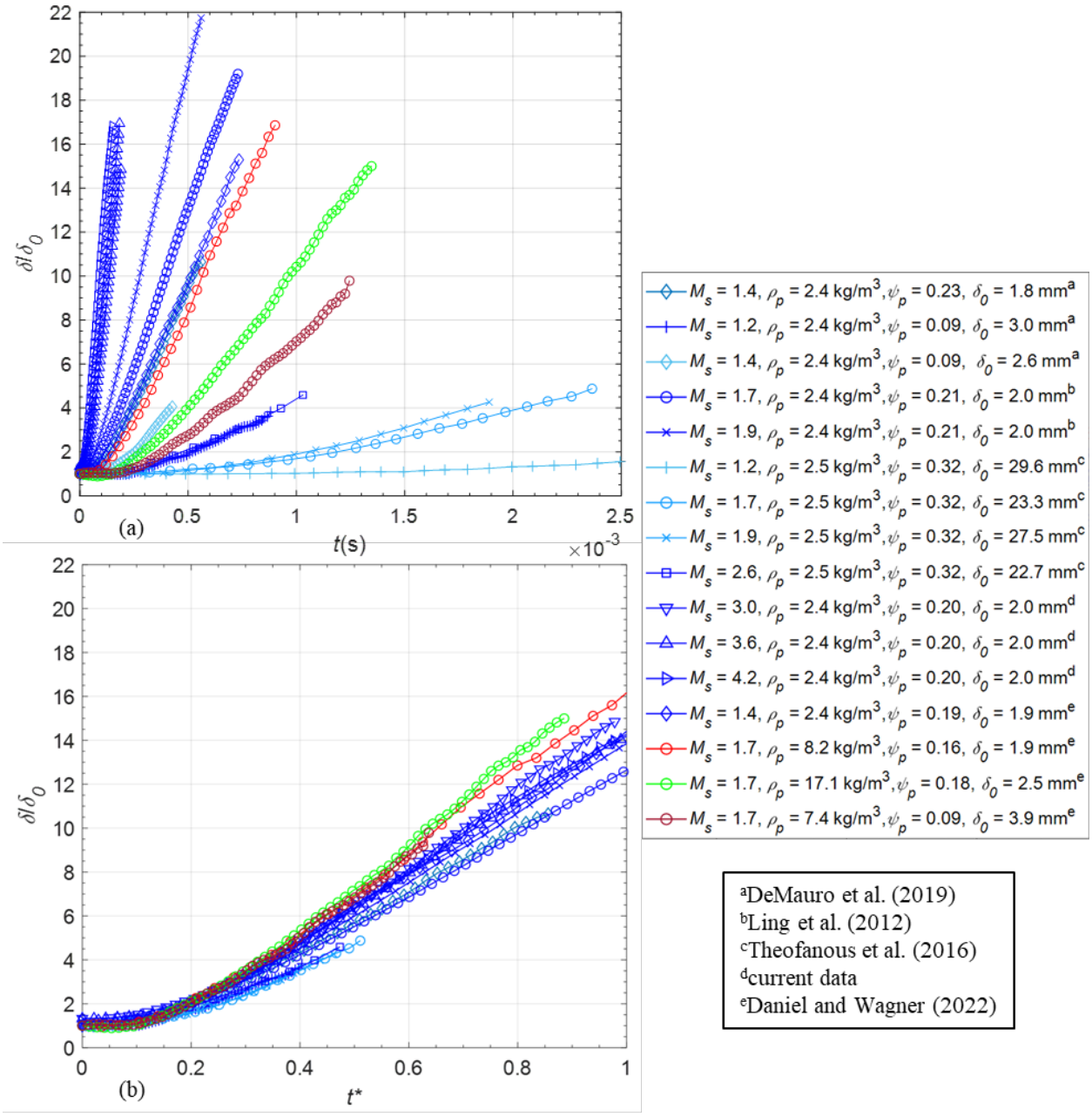

Fig. 6 Comparison of historical particle curtain spread data to current HST results: (a) non-dimensional spread δ/δ_0 versus time, and (b) δ/δ_0 versus t^*. Glass particle trajectories are shown in blue, steel in red, and tungsten in green.